2.1 Introduction

Material synthesis and optimization is an important part of experimental research. To observe a peculiar quantum phenomenon a high-quality single crystal of TI is needed which can be obtained by appropriate method. Also, thin film fabrication using a physical deposition method require to follow basic optimization process and suitable environment to observe the intriguing quantum effects in the laboratory. The detailed synthesis procedure is discussed in this chapter to prepare the single crystals and heterostructures we require. Then, the working principle and experimental arrangements of different characterization tools are described in brief to measure different properties of as prepared systems.

2.2 Material Synthesis Techniques

2.2.1 Modified Bridgeman Technique for Single Crystal Growth

Modified Bridgman method has been used to grow the single crystal samples of TIs [78]. The modified Bridgman method is simple, easy and affordable. All the high purity (99.999%) precursor materials are mixed in stoichiometric ratio and placed in a 12 mm quartz tube. As the TIs are sensitive to moisture and oxygen, all the samples are sealed in evacuated quartz ampoules. These ampoules need to be kept vertically inside the furnace and heated beyond the melting temperature of the material, then slowly cooled from to annealed temperature and finally cooled to room temperature.

Single crystals of 5% Dy doped Bi_2Te_3 were prepared using the melt growth technique. The granules of Bi (99.999%), Te (99.999%) and Dy (99.999%) were mixed in proper stoichiometric ratio and heat-treated at 950 ^oC overnight in a sealed evacuated quartz tube. Then it was cooled from 950^oC to 550^oC at the rate of 5^oC/h and annealed for 72 hours, then cooled down slowly (60^oC/h) to room temperature.

We prepared polycrystalline FeSe by mixing Fe powder and Se granules of high purity in a 1:1 ratio by solid-state reaction method under a high vacuum (10^{-4} mbar). Then, the stoichiometric mixture of high purity (99.999%) Bi and Se granules along with prepared FeSe powder were sealed in quartz ampules under 10^{-4} mbar pressure to prepare $(Bi_2Se_3)_{1-x}(FeSe)_x$ (x = 0, 0.05, 0.1) single crystals. The ampules were heated up to 900 °C and were kept at that temperature for 24 hours and then cooled to 550 °C at the rate of 5 °C per hour to obtain single crystals, which can be cleaved easily along the (00l) plane.

Similarly, to formulate Sb_2Te_3, a stoichiometric combination of Sb (99.999% purity) and Te (99.999% purity) were mixed and vacuum-sealed in a quartz ampoule. The ampoule was placed in a muffle furnace for heat treatment at 900 °C and was annealed at 550 °C for 72 hours followed by a slow cooling rate of 5 °C per hour. In Figure 2.1, the flow chart of the synthesis process and the image of the cleaved single crystal sample are shown.

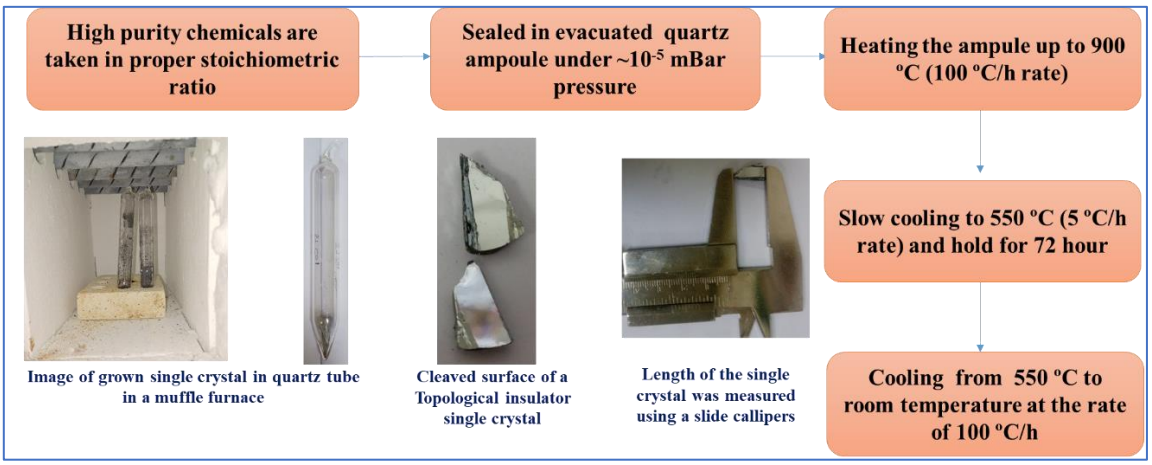

Figure 2.1: Flow-chart of single crystal growth technique using modified Bridgeman method is shown with images taken during the process.

2.2.2 Solid-State Reaction method for Poly crystal Synthesis

Initially, we prepared polycrystalline FeSe by a solid-state reaction where Fe (99.98%) powder and Se (99.999%) granules were mixed in an appropriate stoichiometric ratio and ground thoroughly. The reaction mixture was sealed in an evacuated quartz tube as the chemicals are non-oxide and this was heat-treated for 72 hours at 700 °C, which is the sintering temperature of the material to obtain a pure phase. The flow-chart is displayed in Figure 2.2.

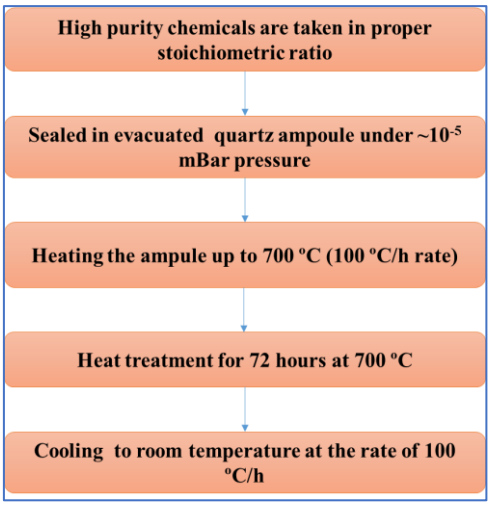

Figure 2.2: Flow-chart to prepare polycrystals using solid-state reaction technique.

2.2.3 Pulsed Laser Deposition (PLD) Technique

PLD is a renounced physical deposition technique where we use KrF excimer gas laser as a laser source. Here, premix gas is used for optical pumping. Under application of high voltage electric discharge, Kr and F are forced to jump to their respective excited states to form an excited dimer called excimer. They regain the ground state immediately after producing a high energetic laser pulse. This immerged laser pulse then incident on the target material in the PLD chamber as shown in the schematic Figure 2.3 (a). Due to immense heating at the laser incident point, the surface evaporation happens on the target (Figure 2.3 (e)) forming plasma. This evaporated charge cloud propagates as plume (Figure 2.3 (d))

and deposited on the cleaned substrate surface (Figure 2.3 (f)). This deposition technique requires appropriate deposition condition such as proper laser energy density, laser pulse rate, chamber pressure, proper gas environment, gas flow rate, substrate temperature, substrate to target distance etc. It is must to calibrate all these parameters for each material for the growth of homogeneous thin films of required thickness.

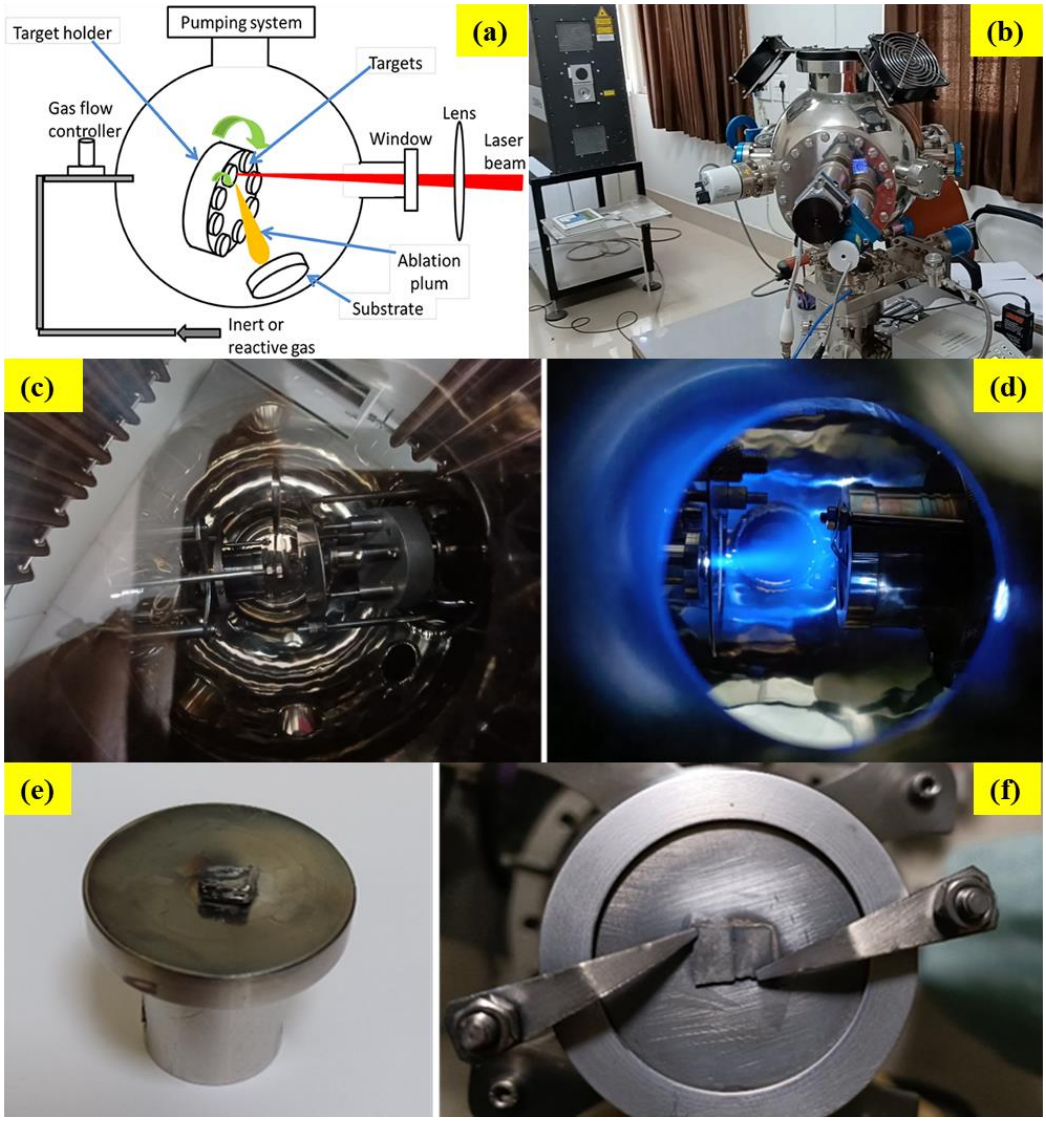

Figure 2.3: (a) Schematic of PLD film fabrication mechanism [79], (b) PLD unit in Department of Physics, IIT (BHU), Varanasi, (c) PLD chamber, (d) PLD chamber when plasma plume is created by a laser pulse, (e) Target material used in PLD, (f) Substrate after deposition.

2.2.3.1 Film Fabrication

Initially, we prepared polycrystalline FeSe by solid-state reaction and formulated Sb_2Te_3, by modified bridgeman technique. The heterostructures of FeSe and Sb_2Te_3 on Si (001) substrate have been prepared using as-prepared FeSe and Sb_2Te_3 as targets by Pulsed Laser Deposition (PLD) technique using a KrF excimer laser under argon environment. In this fabrication process, a Stranski-Krastanov (S-K) type growth [80] has been observed where a significant strain energy per unit area causes nuclei formation over initial 2-D layers. The main reason for this type of growth is substrate-film lattice mismatch, the structural parameters of the used samples are described in Table 2.1 as,

Table 2.1 The structural parameters of the used substrate and target materials.

Material	**Structure**	**A**	**B**	**c**	**α**	**β**	**Γ**
Si substrate	Cubic	5.43Å	5.43Å	5.43Å	90°	90°	90°
Sb_2Te_3 target	Rhombohedral [81]	4.2648Å	4.2648 Å	30.438 Å	90°	90°	120 °
FeSe target	Tetragonal (Refinement result)	3.7694 Å	3.7694 Å	5.5301 Å	90°	90°	90°

Due to this lattice mismatch, as strain energy starts accumulating in the growing film, the 2-D film surface roughens by island formation above a critical thickness. This phenomenon is very much clear in the Field Emission Scanning Electron Microscopy (FESEM) cross-sectional images (Figure 2.4(a-c)): lower the thickness, smoother the surface topography and island formation start above 50-60 nm thickness. Nevertheless, we have noted that a higher substrate temperature and low deposition rate (longer time to form film) yield a more homogeneous film[82]. Thus, we used laser pulse of 3 J/cm^2 energy density and 2 Hz frequency, while substrate temperature was fixed at 300 ºC. The deposition was performed sequentially exposing the respective target material in the pulsed laser.

2.2.3.2 Thickness Calibration for Heterostructure

The thin film deposition rate using PLD corresponding to each material is different depending on its composition, hardness, sintering temperature, etc. Hence, after calibrating deposition parameters like substrate temperature, energy density and frequency of the pulsed laser, we moved forward to calibrate the thickness of the desired system with the number of laser shots while keeping an identical environment. To do so, we have prepared

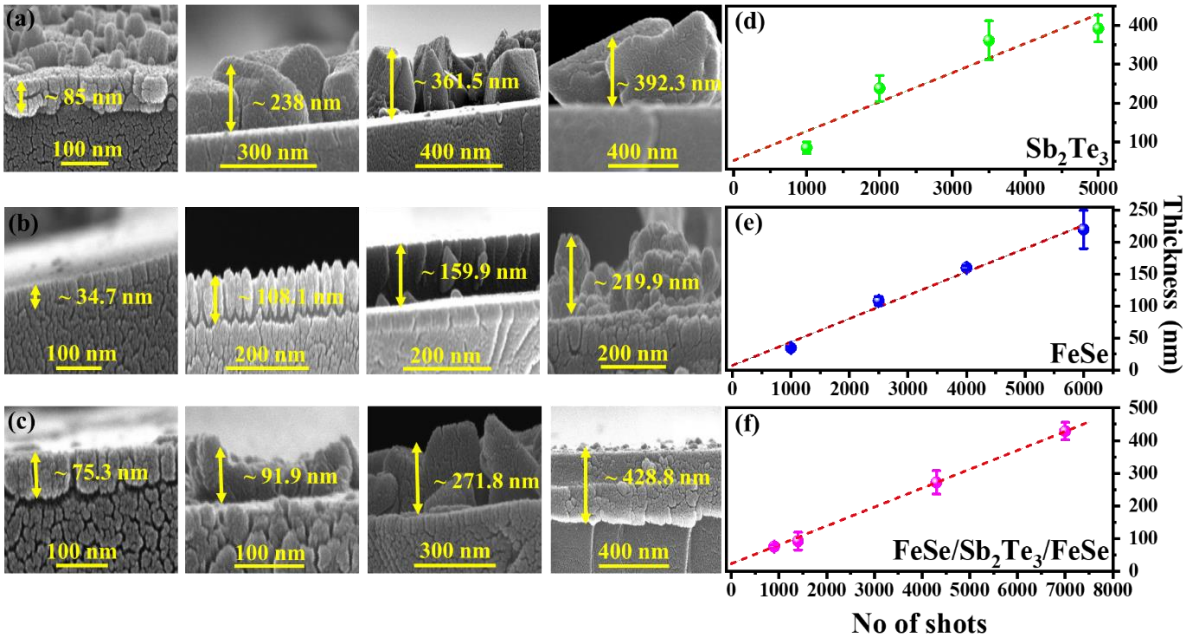

Figure 2.4: The cross-sectional FESEM images corresponding to the (a) Sb_2Te_3, (b) FeSe and (c) FeSe/Sb_2Te_3/FeSe films showing different thicknesses. Thickness vs number of laser shots plotted for (d) Sb_2Te_3, (e) FeSe and (f) FeSe/Sb_2Te_3/FeSe films.

a series of Sb_2Te_3 and FeSe thin films varying the number of laser shots and the thickness was monitored through FESEM cross-sectional images. We plotted the average thickness corresponding to each film against the number of shots as shown in Figure 1.4 (d, e). It was observed that the thickness of Sb_2Te_3 and FeSe films are almost linearly dependent on the number of shots with different slopes of 0.07531 and 0.03653, respectively. Using this calibration, we varied the number of shots to prepare the heterostructures of FeSe/Sb_2Te_3/FeSe, modifying the thickness of each layer. The thickness and number of

shots corresponding to each layer of prepared heterostructures are listed in Table 2. We plotted the average thicknesses (evaluated from the FESEM images) of the heterostructures with respect to the total number of shots as shown in Figure 2.4 (f) which follows linear dependency with each other. As discussed above, due to lattice mismatch, surface roughness starts increasing above a critical thickness for each sample, and also, it is highly likely in the case of heterostructure formation. For this reason, we have kept the thickness of each individual layer below its critical thickness (experimentally optimized). Once the heterostructure is formed, the final roughness does not affect the physical properties of the sample that much. Moreover, when the accumulated strain energy in the films is released, it triggers island formation (sometimes a large one) [83]. It has also been observed in our case that very few islands formed (having a maximum peak of ~ 60 nm) over the film surface.

2.3 Experimental Characterization Tools

2.3.1 X-Ray Diffraction (XRD)

When electromagnetic radiation interacts with a periodic structure, a diffraction phenomenon occurs. X-rays are electromagnetic waves having a very short wavelength of the order of a few angstroms (1 Angstrom = 0.1 nm). The very short wavelength of X-ray denotes the high value of energy. When a monochromatic beam of x-ray is incident on the sample, the incident X-ray photons interact with the electrons of an atom in the sample. As a result, some of the photons are diffracted away from their original incident direction. Diffraction is the phenomenon in which the electromagnetic wave bend forms an obstacle if the obstacle's size is comparable to wave wavelength. In crystalline materials, an inter-atomic distance lies in the range of 1 to 10 Å, which is the same order of X-ray wavelength. The constructive interference occurs only when the interference peaks are observed for a

particular crystalline solid at particular angles. In the crystals, atoms are arranged periodically. Suppose the interference occurred by diffracted waves from the atomic planes satisfies Bragg's condition. In that case, it gives the X-ray diffraction pattern of a given material by measuring the intensity of diffracted waves with a variation of the X-ray incident angle. A lot of information can be obtained from the XRD pattern of the sample, i.e., information about the phase of the synthesized sample and provides the information of crystal structure and the dimension of the unit cell.

W. Lawrence Bragg and William H. Bragg have given law for the diffraction of X-ray from the crystalline planes, known as Bragg's law [44]. Bragg's relation can elucidate the relation between the angle at which the beam diffracts from the crystalline structure and wavelength used for X-rays. The relation can be expressed as:

$$2d\ sin\ \theta\ =\ n\lambda \tag{2.1}$$

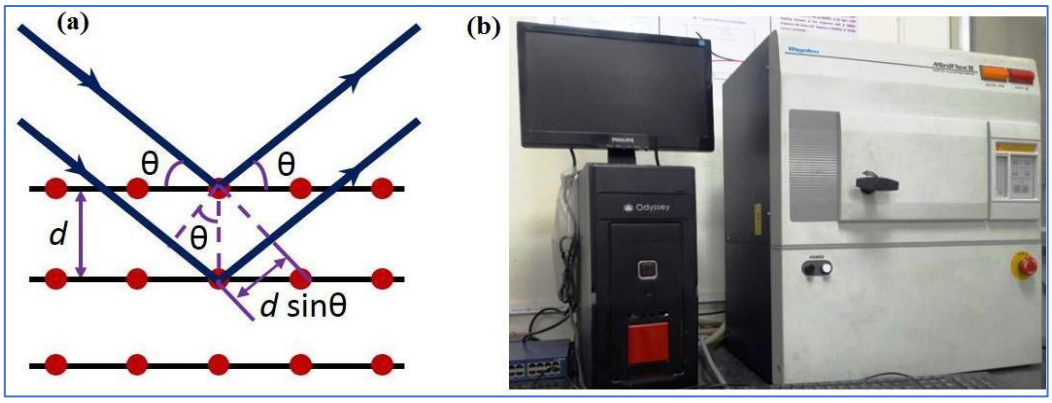

Figure 2.5: (a) Photographic demonstration of Bragg's law (b) Actual photograph of Rigaku Mini Flex II DESKTOP X-ray diffractometer set up.

Where n is an integer representing the order of diffraction, λ is the wavelength of X-ray used, d is the interplanar distance of atoms and θ is the scattering angle or Bragg's angle. The intensity of diffracted X-ray is recorded as a function of the Bragg angle 2θ. The Rigaku-Miniflex II DESKTOP powder X-ray diffractometer, as shown in Figure 2.5, was

used to record the intensity *vs.* 2θ data. This diffractometer has a monochromatic X-ray source with Cu-K_α radiation (λ = 1.5418 Å) at 30 kV and 15 mA.

2.3.2 Transport Properties Measurements

2.3.2.1 Longitudinal Electrical Resistivity (ρ_{xx})

The resistivity of the synthesized single crystal samples was measured using the Quantum Design Physical Property Measurement System (QD-PPMS) by adopting four-probe method. When electrons travel through the crystal, they feel the resistance in their motion. To move the electrons against this resistance, a potential difference is needed to apply across the crystal. According to Ohm's law, if the current *I* flows through the crystal with resistance *R*, then voltage *V* will drop against this resistance through the crystal from equation, $V = IR$. The quantity that characterizes the material is resistivity (ρ_{xx}). The resistivity of a particular material depends on the synthesis process. The resistivity of a crystal is inversely proportional to the length *l* between two voltage probes and proportional to the cross-section area *A*. Mathematically, it can be expressed as:

$$\rho_{xx} = \frac{RA}{l} \tag{2.2}$$

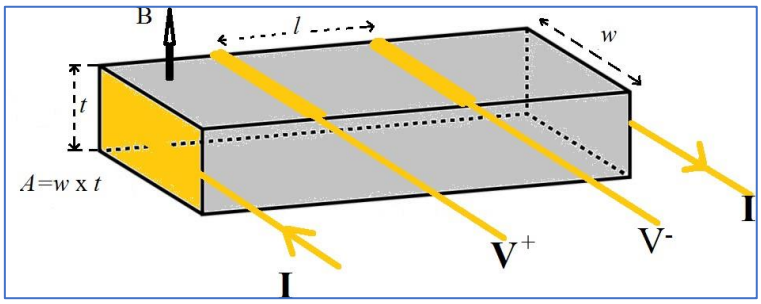

Figure 2.6: Schematic of four-probe measurement geometry.

The resistivity measurements were carried out on a uniform rectangular single crystal sample by employing a conventional four-probe technique between 2 K and 300 K with

(MR) and without (ordinary resistivity) applying external magnetic field B normal to the surface of the sample as shown in Figure 2.6.

2.3.2.2 Transverse Electrical Resistivity (ρ_{xy})

Hall resistivity or the transverse resistivity measurement was also accomplished by using Quantum Design Physical Property Measurement System (QD-PPMS) by changing the connection geometry as displayed in Figure 2.7. In this case, the voltage drop was measured across the opposite surfaces of the sample perpendicular to both current (*I*) and external applied magnetic field (*B*). When a particle of charge q moves perpendicular to B in a current carrying conductor, a Lorentz force $F = qv \times B$ is developed on the charge perpendicular to both the direction of the particle motion and the field. Therefore, the transverse voltage or Hall voltage V_H is measured by applying a fixed longitudinal current *I* across a sample. The graph between measured Hall resistivity ρ_{xy} versus applied magnetic field gives the accurate value of Hall coefficient ($R_H = 1/nq$). A linear variation of ρ_{xy} as a function of field is yielded and the value of R_H is determined from the slope of this linear line. A negative value of R_H indicates n-type nature of charge carriers in a sample, while a positive value of R_H suggests p-type nature of charge carriers. The voltage difference measured between two opposite surfaces provides the value of Hall voltage V_H and the Hall resistivity can be obtained as:

$$\rho_{xx} = \frac{V_H A}{Il} \tag{2.3}$$

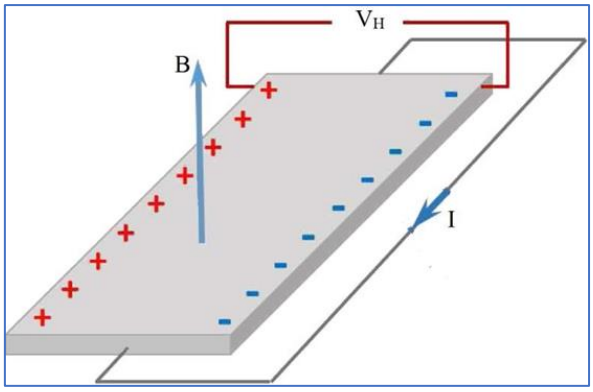

Figure 2.7: Schematic diagram for Hall Effect measurement.

2.3.2.3 Thermoelectric Measurement

The Seebeck coefficient (*S*) was determine by homemade setup in which sample was sandwiched in between two copper blocks. The sample holder assembly was mounted on the close cycle refrigerator (CCR) which was able to cool up to 20 K from room temperature in controlled manner. The temperature difference across the sample was maintained at 2 K with the help of T- Type thermocouple by placing two heater coils at both ends of two copper blocks. The voltage difference (ΔV) between the cold end and the hot end was measured with the help of Keithley 2182A nano-voltmeter from low temperature to the room temperature. The sample holder assembly is illustrated in Figure 2.8. Consequently, there is diffusion of charge carriers from hot end to the cold end, which generates a thermal current. Seebeck coefficient (*S*) is the ratio of magnitude of an induced thermoelectric voltage ΔV with respect to the temperature difference ΔT across the sample, given as:

$$S = \frac{\Delta V}{\Delta T} \tag{2.4}$$

Where, *S* is measured in μV/K and its slope gives the nature of the transport carrier. A negative slope indicates n-type nature of transport carriers in a sample, while the positive slope suggests p-type nature of transport carriers.

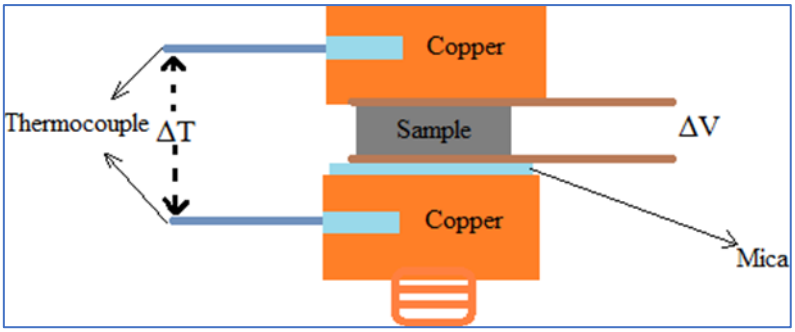

Figure 2.8: Schematic diagram of sample holder for thermoelectric measurement. Temperature difference at the both ends of the sample creates a temperature gradient.

2.3.3 Magnetic Property Measurement System (MPMS)

Quantum Design (QD) MPMS is designed to examine the magnetic properties of small samples over a wide range of magnetic fields and temperatures. This device is able to measure a very small change in the magnetic field with enormous precision. It is controlled by several electronic controllers and provides data collection by a computer. Magnetic measurements are performed by extremely sensitive Superconducting Quantum Interference Device (SQUID). Thus, the MPMS is often called SQUID magnetometer. The QD-MPMS is most widely used to measure the magnetic property through vibrating sample magnetometer (VSM) mode. A solenoid of superconducting wire (Superconducting magnet) is used in MPMS to produce a magnetic field up to ±7 Tesla (±70 kOe). The superconducting magnet and SQUID detector are both cooled by liquid helium. The sample chamber is cooled by the combination of both liquid nitrogen and liquid helium. MPMS covers the large temperature range measurement from 2 K – 800 K with magnetization measurement sensitivity of 5×10^{-8} emu. In SQUID VSM, sample vibrates sinusoidally with the frequency ω about the center of the detection coils, where the signal picks as a function of the sample *Z(t)* position. Therefore, the expression for generated SQUID signal *V(t)* as a function of time t can be given as:

$$Z(t) = Sin(\omega t) \tag{2.5}$$

$$\text{And } V(t) = A\,Z^2(t) \tag{2.6}$$

$$V(t) = AB^2 sin^2(\omega t) \tag{2.7}$$

Here, *A* is a scaling factor relating to the magnetic moment of the sample and B is the sample vibration amplitude. In this system, the SQUID works as an extremely sensitive current to voltage converter and is inductively coupled with the detection coil. Basically, the SQUID functioning is based on Josephson tunneling effect and flux quantization in superconducting ring. Due to vibration of the magnetic sample through the coils, the coils generate the current in response to the disturbance in a local magnetic field. The SQUID feedback nulls the current in the pickup coils, so basically, there is no flow of current in them. Hence the SQUID voltage corresponds to the feedback current gives the value of sample magnetization. All the magnetic measurements of the present thesis are performed by QD-MPMS-SQUID-VSM, which is shown in figure 2.9.

2.3.3.1 DC Magnetization and AC Susceptibility

To perform dc and ac magnetization measurements, mainly five major protocols are followed viz.

• Zero-field-cooled heating (ZFC): This protocol is followed when the sample is cooled from the room temperature to the lowest temperature of measurement with zero magnetic field. After switching on a required magnetic field, the data are recorded when the sample heated to the desired T.

• Field-cooling (FC): FC condition is done by cooling the sample down to the lowest T of measurement from room temperature in the presence of a magnetic field. M(T) data are recorded during the cooling cycle.

• Field-cooled heating (FCH): After obtaining FC condition, FCH protocol is followed by recording the data during heating in the presence of a magnetic field. MH measurement: MH-curves ae hysteresis curves which are measured at constant T and here the magnetic field increases or decreases slowly which does not affect the dynamical magnetization processes.

• AC Susceptibility: Apart from above mentioned dc measurements, the real and the imaginary part of ac susceptibility (χ' and χ'' respectively) are also measured using the same instruments with varied T and f.

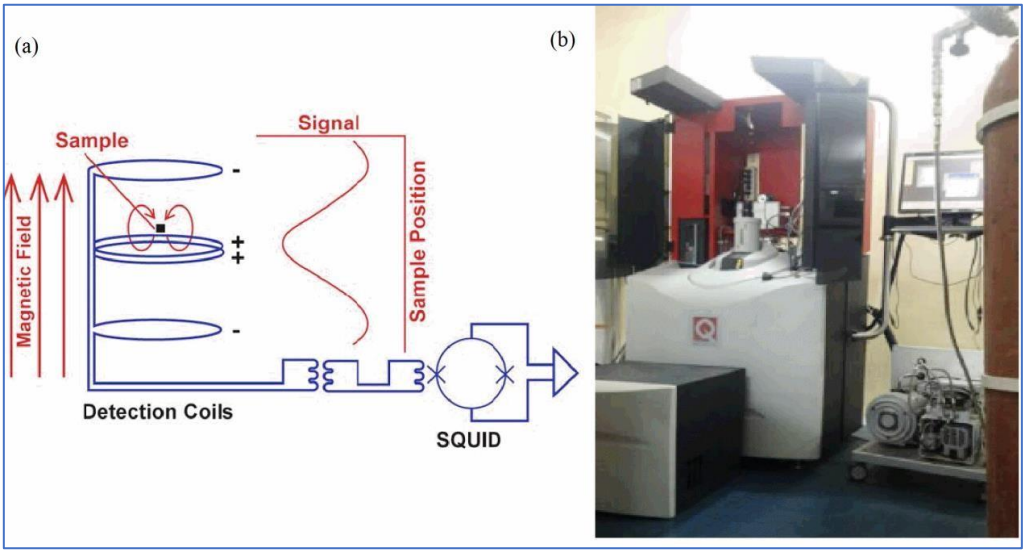

Figure 2.9: (a) Schematic diagram of SQUID-VSM detection system. (b) Photograph of actual QD-MPMS measurement system.

2.3.4 Raman Spectroscopy

The "Raman spectroscopy" is based on the scattering of light through a matter. Historically, after the discovery of Compton scattering in 1923, where X-ray is scattered by electrons and the wavelength of the X-ray is changed, C. V. Raman though the optical analogue of Compton effect and ultimately in 1928, Raman with his research partner Krishan was able to discover the Raman spectroscopy. When Raman did his first, he used sunlight as a source and his naked eye as a detector, due to unavailability of advanced

instrumentation. Afterwards, the light was allowed to fall on a photographic plate. Later on, a lot of improvements have been made like invention of a good excitation source with advanced detector and a commercial Raman spectrometer was accessible. And this spectroscopy become an innovating technique to probe the qualitative and quantitative dynamic of atoms/ions/molecules in crystal using the scattering of light. While light scattering from the molecule/crystal, the most of photons get elastically scattered. The elastically scattered photons will possess the same energy as the incident photons. There is a very small fraction of light (~1 photon out of 107 photons) which gets inelastically scattered with a change in their wavelengths by changing by changing rotational/vibrational/electronic energy of the molecule. This inelastic scattering is known as the famous Raman Effect (i.e., usually described as Raman shift) and the elastic scattering is recognized as Rayleigh scattering. The phenomena of Raman effect can be explained based on the deformation of molecules in an electric field of strength *E* owing to the induced electric dipole moment, $P = \alpha E$ (α is the polarizability). The Raman shift can be observed only the derivative of α is nonzero with respect to Q (normal co-ordinates). When electromagnetic adiation interacts with the atom/molecule the electron clouds and bonds of the molecules get distorted. Due to this interaction, the atom/molecule get excited to a virtual energy state from their ground state thus becomes unstable. These excited molecules return to a different stable state (rotational or vibrational) by decreasing their energy through releasing a photon. The difference in energy of initial stable state of and final stable of the molecule cause shifting of the frequency of the emitted photon from the excitation energy. If the final state has large energy, then the we get an emitted photon of a lower frequency than the excitation frequency and this shifting of energy of scattered photon is known as stoke shift (Figure 2.10 (a)). However, when the final state has lesser energy then we get an emitted photon higher energy and this shifting is nominated as Anti

Stokes shift. The Raman spectra are usually described in terms of wave numbers in the units of inverse of length (cm^{-1}). In our study, we have used Renishaw Raman spectrometer, which is shown in Figure 2.10 (b). Here, a monochromatic laser light of wavelength 532 nm, using diode-pumped solid-state laser with a maximum power of 100 mW was used. To avoid heating of the specimen, only 5% power was allowed to incident on the sample. The laser beam was focus at a much shorter working distance over a 50 × long-distance objective connected with the Leica DM 2500M microscope. A dispersion grating with 2400 groves/mm with 50 micron slit width has been used to keep the constant phase throughout the experiments. The scattered light has been collected and passed to a detector. The data was collected using the supplied 4.0 software Spectrometer scanning and finally processing of data was finished.

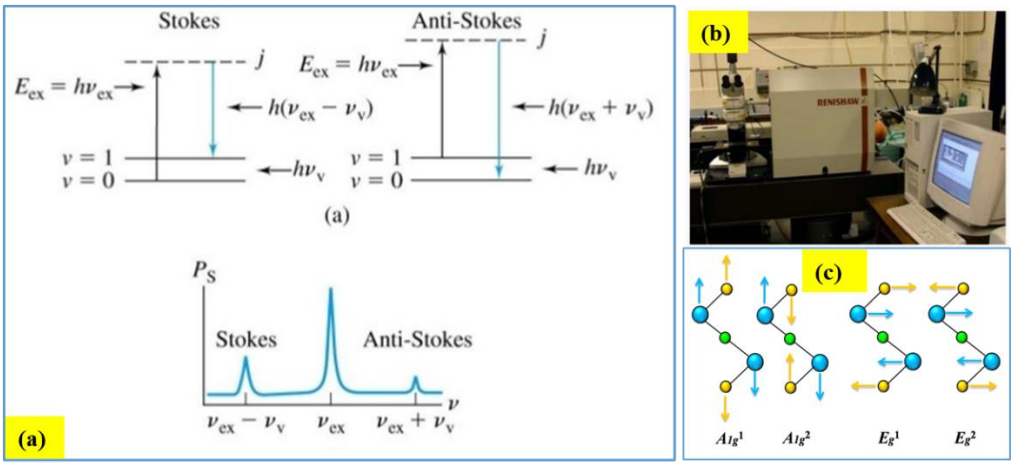

Figure 2.10: (a) Illustration of Raman effect using energy level diagram [84]. (b) Display the picture of Renishaw micro-Raman spectroscope used in our characterization. (c) Vibrational Raman modes corresponding to Sb_2Te_3 single crystal.

We have used the temperature dependent Raman spectroscopy technique (LabRam HR evolution spectrometer, maker: Horiba) to demonstrate the vibrational modes and how they modify depending on magnetic ordering or structural deformation. Here longitudinal and transverse vibrational Raman modes corresponding to a basic TI Sb_2Te_3 is shown using its atomic configurations.

2.3.5 X-Ray Photoemission Spectroscopy (XPS)

The XPS which is also called photoelectron spectroscopy for Chemical Analysis (ESCA), is a powerful technique used to collect chemical information about the surfaces of solid materials *viz*., oxidation states, elemental composition, ligand coordination, etc. Both the insulators and conductors can easily be investigated in surface areas from a few microns to a few millimeters in depth. In fact, the XPS is used as a surface-sensitive tool since it mainly identifies those electrons produced near the surface. The photoelectrons of interest have comparatively small kinetic energy. As a consequence of the inelastic collisions in the sample's atomic structure, photoelectrons producing more than 20 to 50 Å beneath the surface cannot escape with sufficient energy to be detected in this technique.

The sample under investigation is kept inside an ultrahigh vacuum ambiance (typically ~10-10 torr) and then it is exposed to a monochromatic, low-energy X-ray source. The X-rays incident on the sample results in the ejection of core-level electrons from sample atoms. In fact, the energy of a core electron produced in such a photoemission process is a function of its binding energy and is a characteristic of the element from which it was emitted. As a matter of act, the primary data used for XPS is the energy analysis of the photo-emitted electrons. When the incident X-ray ejects the core electron, an outer electron fills the core hole. By the emission of an Auger electron or a characteristic X-ray, these energies get compensated. Further, in XPS Auger electron's energy can also be utilized along with the emitted photoelectrons. The following equation is used for the energy of each of the photoelectrons which is purposed by Ernest-Rutherford (1914):

$$E_{\text{kintetic energy}} = h\nu - (E_B + \phi) \tag{2.8}$$

Here, E_B represents the binding energy of the electron, $h\nu$ represents the energy of the incident X-ray photons being used, $E_{\text{Kinetic energy}}$ represents the kinetic energy of the electron

that is measured by the spectrometer and the work function of the spectrometer is known as ϕ. This is illustrated in the schematic diagram Figure 2.11 (a). The different instrumental units of an XPS machine as demonstrated in the schematic Figure 2.11 (b) as,

1. Hemispherical electron energy analyzer
2. X-ray source
3. Ar-ion gun
4. Vacuum system
5. Neutralizer or electron flood gun
6. Multi-channel detector plates
7. Sample stage or holder
8. Electronic control units
9. Computer

X-ray photoemission spectroscopy (XPS) technique was used for our systems to understand the elemental valance states of the single crystals and how they modify for the as-prepared films. The Al-Kα X-ray source and the analytical aperture of diameter 400 μm were used to measure the depth profile over the 2 mm × 4 mm area of the heterostructure by sputtering of 1 keV argon ions. The neutralizer attached to the XPS instrument was used for charge compensation, and the neutralized condition was uniform in both sputtering and measuring XPS spectra.

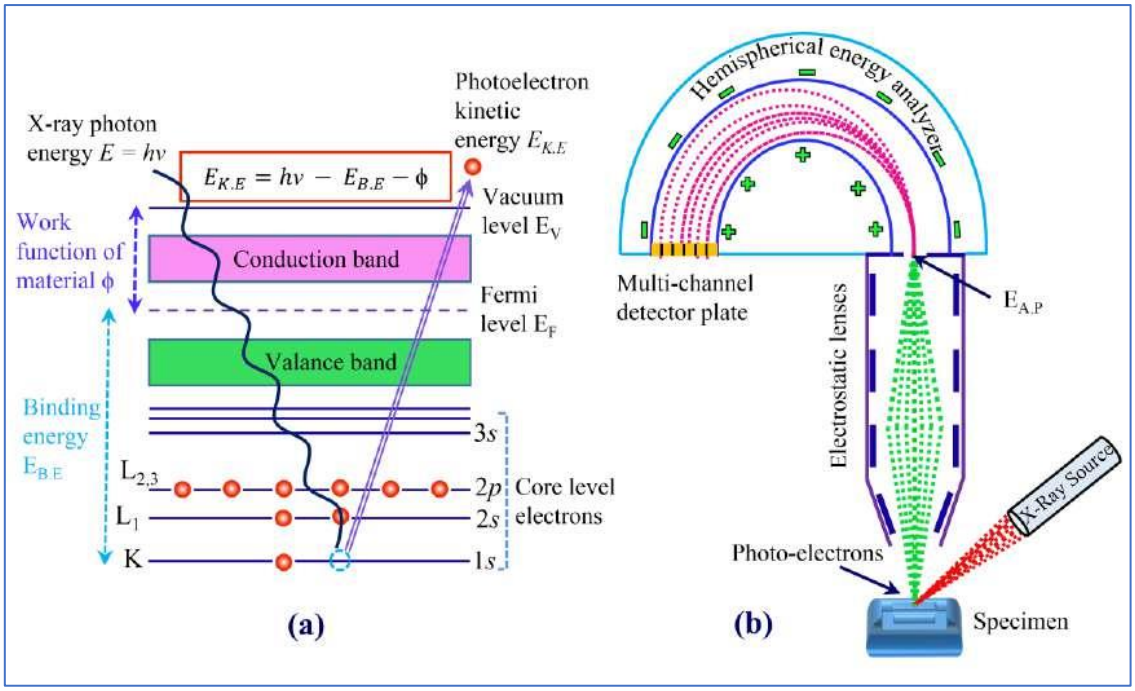

Figure 2.11: (a) Schematic diagram of a core-level-photoelectron emission process. (b) Hemispherical electron energy analyzer [85].

2.3.6 Scanning Electron Microscope (SEM)

Scanning electron microscopy, abbreviated as "SEM," is one of the most useful characterization tools available, which provides a magnified image of an object by focusing a stream of electrons on scanning its surface for a high-resolution image. It provides details on both man-made and naturally existing materials' topography, chemical composition, and microstructure morphology. The adaptability of SEM is advantageous for a plethora of scientific, research, industrial, and commercial applications, including biology, forensics, medicine, electronics, and materials science.

SEM uses comparatively low intensity, focused electron beam as an electron probe that periodically scans across the sample. SEMs are a form of electron microscope used for the in-depth study of solid object surfaces. Major elements of a conventional SEM's column structure include:

1. Electric source

2. Electron lenses (Condenser and objective)

3. Apertures

4. Scan coils

5. Detectors (different for secondary electrons (SEs) and back scattered electrons (BSEs))

In scanning electron microscopy, the sample is scanned by the electron beams that is produced at the tip of the column, driven downward, and then focused into a beam that reaches the sample's surface after passing through a number of lenses and apertures. As a sample is positioned on a stage in the chamber region, the chamber and column are both evacuated using a variety of pumps.

Figure 2.12 shows that scan coils located above the objective lens govern where the electron beam will impact the material. The sample's surface may be scanned by the beam due to these coils. Data can be collected on a specific region of the sample using this beam scanning. Several signals are produced as a result of the electron's interaction with the material is necessary for image creation in the SEM. The proper detectors are used to find the signals. BSEs were created in the sample's deeper regions, which revealed information on the sample's topography and composition. SEs come from areas near the surface. As a result, it provides topographic contrast information with high resolution for the observation of surface texture and roughness. By putting them on carbon tape, the majority of nanomaterials (conductive in nature) can be directly viewed by SEM. Metal coatings (gold, silver, platinum, etc.) are required for non-conductive samples (bioorganic nanomaterials).

We have studied FESEM images on the sample surface to understand the morphology of our system exhibiting grain size for films and layer thickness for single crystals. Also, cross-sectional FESEM image was incorporated to measure the thickness of as prepared thin film and heterostructures in present thesis.

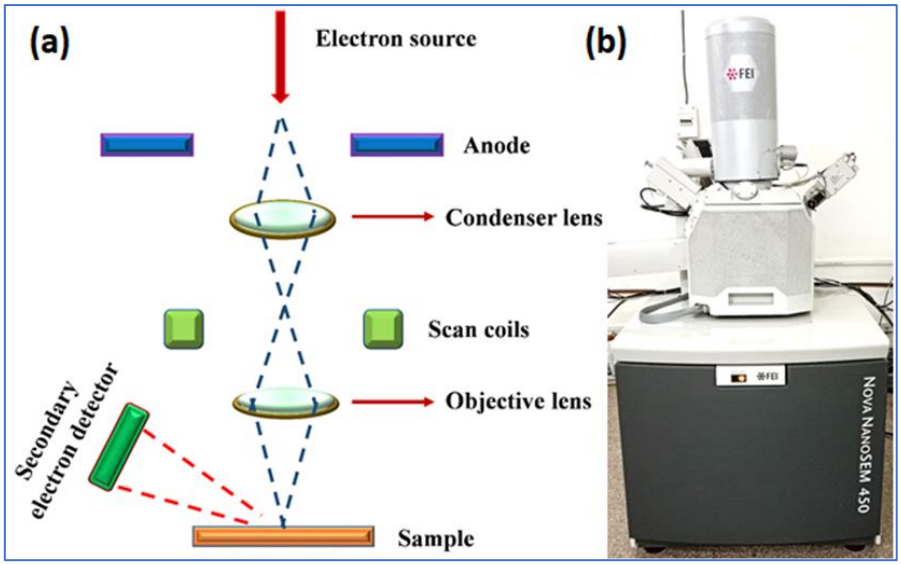

Figure 2.12: (a) Scanning electron microscope' Schematic presentation [86]. (b) Scanning electron microscope (FEI NOVA NANO SEM 450, Courtesy CIFC IIT BHU).

2.3.7 Energy-Dispersive X-ray Spectroscopy (EDS)

EDS is a powerful tool for identifying a specimen's elemental composition. Commonly, an EDS detector is integrated with an SEM system; EDS functions by detecting the characteristic X-ray specific to each element. As discussed above, the bombardment of a high-energy electron beam leads to a significant probability of X-rays generation too, which is detected by mounted EDS detectors. Using this technique, one can detect the presence of a particular element in a material. Generally, bombarded electrons go through the inelastic scattering from the atomic electrons and may lead to the ionization of atoms in which core-level electron is most probable to eject. For stability, higher-level electrons jump to the vacant place, generating a characteristic X-ray of specific energy, *i.e.*, equal to the energy difference of two levels. These characteristic X-rays are lament-specific, which earns detecting them reveals the identity of elements present in the specimen. The de-acceleration of the electrons in the atomic field also generates the continuum X-rays, so-called Bremsstrahlung radiation. Thus, a typical Xray spectrum contains sharp X-ray peaks and some background radiation. Thus, the major drawback of X-ray detection is that the X-

ray reached by the detector is not only a characteristic X-ray. The Bremsstrahlung X-rays are emitted continuously over the range of the energy spectrum. The characteristic X-ray in an EDS spectrum is always superimposed over Bremsstrahlung radiation that behaves as a background. Nevertheless, the angular distribution of Bremsstrahlung radiation is a robust forward peak. Hence, the X-ray detector is mounted at a more significant scattering angle, restricting the bremsstrahlung background from swamping the characteristic Xray. In this thesis, the EDS characterization has been performed in Helios Nano Lab™ 600i instrument (M/s FEI Quanta, Switzerland) equipped with an EDS detector from EDAX/AMETEK and M/s Inca X-act EDS detector.

2.3.8 Atomic Force Microscopy (AFM)

AFM is a very high-resolution scanning probe microscopy (SPM) with a demonstrated resolution in the nanometer range. AFM has usually been utilized to measure the roughness of the sample surface at a very high resolution [87]–[89]. The AFM consists of a cantilever with a sharp tip (probe) at its end that scans the sample surface. The cantilever is typically made of silicon or silicon nitride with a tip radius of curvature in the nanometer range. According to Hooke's law, when the tip is brought into proximity to a sample surface, interatomic forces between the surface atoms of the sample and the tip led to a deflection of the cantilever. Depending on the measuring conditions, forces that are usually measured in AFM include van der Waals forces, mechanical contact forces, chemical bonding, capillary forces, electrostatic forces, and magnetic forces. Moreover, specialized probes may concurrently measure additional properties. Typically, the deflection is measured utilizing a laser spot reflected from the top of the cantilever into a collection of photodiodes. The beam Bounce method is being used for the detection of the cantilever deflection. The laser light incidents on the reflecting back surface of the cantilever tip and then the spot incidents on the Position Sensitive Photo Diode (PSPD). As the photodiode is generally

highly position-sensitive, slight deflection of the laser spot on the diode generates some voltage, and thus it detects the deflection. After alignment of the instrument, if the cantilever deflects due to its flexibility, the deflection is noted on the PSPD. However, the z-scanner can move in X, Y, and Z directions. So, the scanner consisting of the cantilever tip moves over the sample surface in a back-and-forth direction again and again to record the data (Figure 2.4 (a)). This way, the piezo scanner scans the sample surface by recording the vertical positions as the tip is rastered across the surface and provides a topographical image [87].

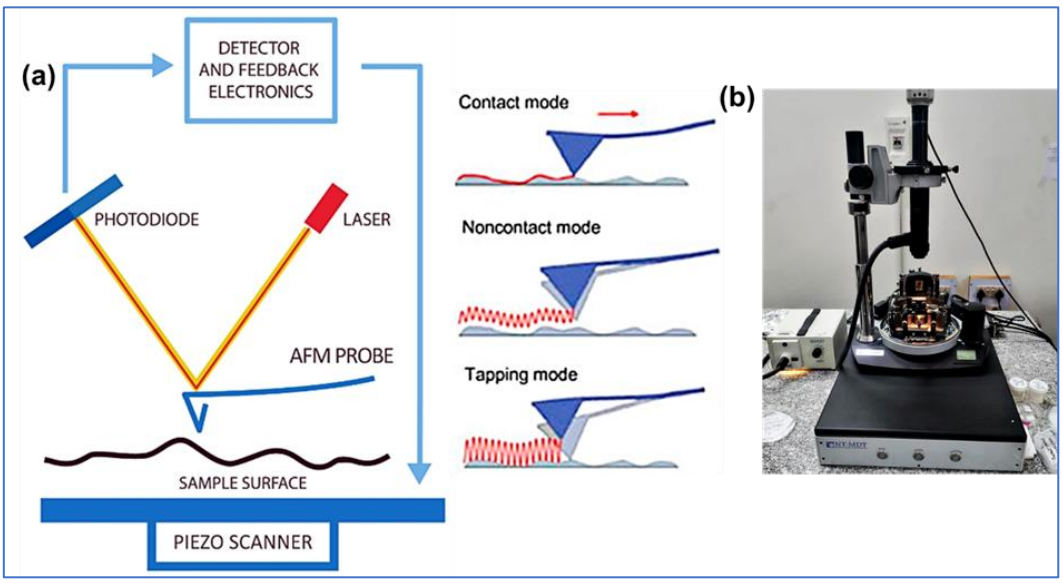

Figure 2.13: (a) The schematic arrangements of AFM along with different probing techniques [87], (b) real image of AFM, NT-MDT Russia.

Different scanning modes are used to probe the force scanning the sample surface:

Contact mode: AFM tip makes soft "physical contact" with the sample surface as the scanner gently traces the tip across the sample.

Non-contact mode: The scan is performed by lifting the probe by at least one nanometer from the sample surface

Intermittent contact mode (tapping mode): This imaging method is similar to contact mode. But, in this mode, the cantilever oscillates at its resonant frequency and gently "taps" on the sample surface during scanning, thus contacting the sample surface at the bottom of its swing. A constant tip-sample interaction is maintained by maintaining a constant oscillation amplitude, and a digitized image of the sample surface is thus gained.

We have carried out AFM over all the prepared thin films to probe the topography and the average roughness on the sample surface and evaluated all the related statistical parameters. Also, magnetic force microscopy (MFM) was measured using magnetic tip to show if there is any magnetic ordering or magnetic domains present in our sample at room temperature.